Porosity and Mechanical Properties of Mesoporous Thin Films Assessed by Environmental Ellipsometric Porosimetry

ARTICLE *in* LANGMUIR · JANUARY 2006

Impact Factor: 4.46 · DOI: 10.1021/la050981z · Source: PubMed

6 AUTHORS, INCLUDING:

Cedric Boissiere
Pierre and Marie Curie University - Paris 6
220 PUBLICATIONS **5,369** CITATIONS
SEE PROFILE

David Grosso
Collège de France
207 PUBLICATIONS **8,695** CITATIONS
SEE PROFILE

Clément Sanchez
college DE france , Pierre and Marie Curie Uni…
600 PUBLICATIONS **25,505** CITATIONS
SEE PROFILE

Porosity and Mechanical Properties of Mesoporous Thin Films Assessed by Environmental Ellipsometric Porosimetry

Cédric Boissiere,[†] David Grosso,[†] Sophie Lepoutre,[†] Lionel Nicole,[†] Aline Brunet Bruneau,[‡] and Clément Sanchez*,[†]

Laboratoire de Chimie de la Matière Condensée, Université Pierre et Marie Curie, 4 Place Jussieu, 75252 Paris, Cedex 5, France, and Institut des Nanosciences de Paris, UMR CNRS 7601, Universite Paris 6, Campus Boussicaut, 140 Rue Lourmel, 75015 Paris, France

Received April 13, 2005. In Final Form: July 22, 2005

Mesoordered silica thin films with cubic structures were prepared by evaporation induced self-assembly (EISA) with two types of structuring agent (CTAB and block copolymer F127). A complete and accurate description of these films was obtained by combining 2D-SAXS analyses, variable angle spectroscopic ellipsometry, and a specially designed environmental ellipsometric porosimetry (EEP) experiment. The EEP analysis is rapid and cheap and operates at ambient pressure and temperature. This latter experiment was performed with water and produced a set of water adsorption−desorption isotherms. A modified Kelvin equation, coupled with a modelisation of pores contraction, enabled the determination of the structural parameters of films porous networks: ellipsoidal pore diameters, porous volume, and surface area. Young moduli of films in the direction perpendicular to the substrates were calculated from these parameters.

Introduction

Porous thin films (typically thinner than 2 microns) are having more and more importance in modern material science due to their numerous high added value applications in energy transfer devices, microelectronic low dielectric constant films, or selective sensors.[1−4] For several years, a growing effort has been made to develop new simple, rapid, non destructive and reliable techniques allowing the characterization of the porous structure of films for industrial production controls and laboratory investigations. Ellipsometric Porosimetry (EP), first reported by Baklanov and co-workers in 2000,[5,6] is a very powerful technique for micro- and mesopores characterization of supported porous thin films. This technique consists of plotting an adsorption−desorption isotherm from the variations of film refractive index induced by the change of partial pressure of an organic solvent above a film. The device is usually based on the coupling of a pressure controlled chamber (conventional in gas volumetry characterization devices) and a spectroscopic ellipsometer. Pore size distribution of micro- and mesopores of the film can then be directly obtained via porosimetry models usually based on the Kelvin equation for the determination of mesopores sizes[5] or different models such as the Dubinin Raduchkevich (DR) model for the determination of micropores sizes.[7] In industry, EP devices are more and more used for quality control of high technology micro- and mesoporous inorganic or hybrid films (such as flat computer screens and low-k layers in microelectronic). Surprisingly, so far, the only EP device available is commercialized by SOPRA Co.[8] In academic and applied research, EP was first used for the characterization of amorphous porous thin layers, and rapidly extended to the determination of the pore size distribution (PSD) of thin layers of mesostructured silica[9] and of organically modified silica films produced by the evaporation induced self-assembly (EISA) process.[1] For porous silica films, spectroscopic infrared ellipsometry gives very useful supplementary information on a film chemical composition.[10]

So far, the accuracy of the EP technique has been limited by two categories of problems. The first limitation comes from the assumption that an adsorbate in confined environments retains its bulk properties (polarizability, volume, and surface tension). The error introduced here depends a lot on both the adsorbate and the chemical surface to be analyzed.[11,12] The higher the polarizabilities of adsorbate and surface, the larger the distortion induced by the porous confinement on the above-mentioned properties. The second limitation is that, so far, porosimetry models used with the EP technique are directly inherited from powder volumetry techniques and are not entirely adapted to films specificities. In these models, the geometry of pores is often assumed to be cylindrical or spherical. For mesostructured films, the unidirectional pore shrinkage associated to the drying and treatment

* To whom correspondence should be addressed. Phone: 00 33 1 44 27 55 42. E-mail: clems@ccr.jussieu.fr.

[†] Université Pierre et Marie Curie, Jussieu.

[‡] Université Pierre et Marie Curie, Boussicaut.

(1) De Theije, F. K.; Balkenende, A. R.; Verheijen, M. A.; Baklanov, M. R.; Mogilnikov, K. P.; Furukawa, Y. *J. Phys. Chem. B* **2003**, *107*, 4280.

(2) Innocenzi, P.; Martucci, A.; Guglielmi, M.; Bearzotti, A.; Traversa, E.; Pivin, J. C. *J. Eur. Ceram. Soc.* **2001**, *21* (10−11), 1985.

(3) Gimon-Kinsel, M. E.; Balkus, K. J., Jr. *Microporous Mesoporous Mater.* **1999**, *28* (1), 113.

(4) Nicole, L.; Boissière, C.; Grosso, D.; Hesemann, P.; Moreau, J.; Sanchez, C. *Chem. Commun.* **2004**, 2312.

(5) Baklanov, M. R.; Mogilnikov, K. P.; Polovinkin, V. G.; Dultsev, F. N. *J. Vac. Sci. Technol. B* **2000**, *18* (3), 1385.

(6) Baklanov, M. R.; Mogilnikov, K. P. *Mater. Res. Soc.* **2001**, *616*, D4.2.1.

(7) Dultsev, F. N. *Thin Solid Films* **2004**, *458*, 137.

(8) SOPRA; Optical solutions: Bois-Colombes, France. www.sopra-sa.com.

(9) Bourgeois, A.; Bruneau, A. B.; Fisson, S.; Demarets, B.; Grosso, D.; Cagnol, F.; Sanchez, C.; Rivory, J. *Thin Solid Films* **2004**, *447*, 46.

(10) Brunet-Bruneau, A.; Besson, S.; Gacoin, T.; Boilot, J. P.; Rivory, J. *Thin Solid Films* **2004**, *447*, 51.

(11) Gregg, S. J.; Sing, K. S. W. *Adsorption, surface area and Porosity*; Harcourt Brace and Co.: Orlando, FL, 1997.

(12) Boissière, C.; Brubach, J. B.; Mermet, A.; de Marzi, G.; Bourgaux, C.; Prouzet, E.; Roy, P. *J. Phys. Chem. B* **2002**, *106*, 1032.

10.1021/la050981z CCC: $30.25
Published on Web 00/00/0000 PAGE EST: 10

lead to nonsymmetrical models. PSD assuming spherical geometry is thus not accurate. Moreover, the pore surface wettability is usually assumed to be perfect in Kelvin methods and is thus usually not taken into account.[11] Since wettability is a crucial factor of the capillary condensation, we will show here that the liquid−solid contact angle, characterizing the surface energy, is needed to give a correct interpretation of the water adsorption−desorption isotherm.

The goal of this work is to develop a simple, general and reliable analytic approach, allowing direct characterization of mesoporous layers (including EISA processed layers) that takes into account pore geometry, pore size, surface area, porous volume, and mechanical properties (usually the stiffness and/or the Young modulus). Thus, we concomitantly report the development of the first environmental ellipsometric porosimetry (EEP) device designed to allow fast film characterization at ambient pressure and temperature. To make mesopore size investigation simple, cheap, and non toxic, we performed EEP measurements using a pulsed air flow with controlled partial pressure of water. This system allows a fast partial pressure equilibration at each point of the isotherm (a complete adsorption−desorption cycle can be obtained within 40 min time), whereas the actual commercial EPs with sealed vacuum chamber have to work with a gradient of absolute pressure (preventing equilibration) to obtain fast measurements. To validate the porous network characterization with EEP, we used mesoporous films made by EISA with known mesoporous networks as test materials. Indeed one can control their structure at many different levels: (i) meso-ordered pore size can be tuned between 2 and 30 nm, (ii) periodical order of the porous network can be either 2D or 3D, (iii) the inorganic wall composition is tunable, and (iv) wall can be either amorphous or nanocrystalline. Thus, one can modulate their chemical and physical properties in a very wide range.[13−20] Two silica films with cubical ordered mesostructures were used. To improve the EP method, a precise analysis of film contractions was performed via the combination of 2D small-angle X-ray scattering (2D-SAXS), ellipsometry, transmission electronic microscopy (TEM), and EEP analyses. A model was introduced to take into account the uniaxial contraction of the inorganic network during thermal treatments which transforms the spherical shape of cubic mesostructured domains into ellipsoidal pores. Calculating the anisotropy of these pores and reintroducing the liquid−solid contact angle allowed us to produce a better modified Kelvin equation for pore size determination and to rationalize some capillary condensation domain shifts due to the evolutions of adsorbate/surface interactions. Finally, we studied and discussed here the influence of pore anisotropy on Young modulus determination.

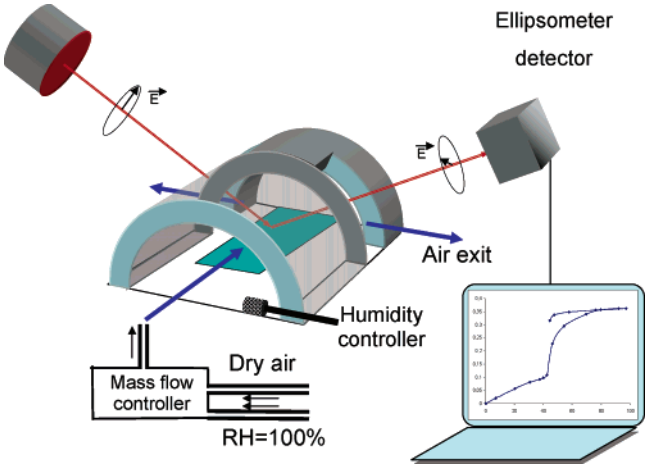

Figure 1. Scheme of experimental ellipsoporometer.

Experimental Section

Silica films with cubic *Pm*3*n* and *Im*3*m* ordered mesostructures were prepared, as reported previously, in the presence of cethyltrimethylammonium bromide (CTAB) or F127 Pluronic block copolymer as structuring agents.[19,21] Solutions were prepared for dip-coating with a molar composition of 1 TEOS: 40 EtOH: 5 H_2O: 0.15 HCl: 0.14 CTAB (or 4×10^{-3} F127 respectively) and aged at 80 °C for 20 min. All products were purchased from Sigma/Aldrich and used as furnished. Thin films were prepared by dip coating silicon wafers of thickness 8 μm (for 2D-SAXS measurements) and one side polished 350 μm thick for EEP experiments. Films were dip coated at a withdrawal speed of 2.7 mm s^{-1} and left for rest 10 min in a 50% relative humidity (RH) atmosphere. This experimental protocol was followed to obtain films with cubic mesostructures, optical homogeneity, and transparency.

They were then kept in sealed flasks at 100 °C at least 1 day before calcination in air at 500 °C for 10 min (5°/min gradient). The removing of organic parts by calcination led to ordered mesoporous silica films with monodisperse pores having different sizes. 2D-SAXS measurements were performed with third generation synchrotron radiations (SAXS beam line of ELETTRA, Trieste, Italy). Ellipsometry measurements were performed on a UV−visible (from 240 to 1000 nm) Variable Angle Spectroscopic Ellipsometer (VASE) from Woolam, and the data analysis was performed with the WVase32 software. The two types of periodically organized mesoporous networks prepared were named accordingly with the structuring agent name and the calcination temperature *T*. Hence, silica films produced from CTAB and silica are labeled **CS-T**, and those produced with block copolymer F127 and silica are labeled **FS-T**. Transmission electronic microscopy (TEM) pictures were obtained with a JEOL CX/STEM. EEP produced adsorption−desorption isotherms were analyzed via the IIC pore contraction model and a modified Kelvin equation (vide infra).

The EEP setup used is represented in Figure 1. It is made of the previously described ellipsometer on which is fixed a cell of environment control containing the film to analyze. In laboratories, gas volumetry analyses are usually time-consuming, mainly because of long pressure equilibration time within the analysis chamber. In the experimental setup of these experiments, we replaced the pressure equilibration system by a continuous flux of air containing a fixed partial pressure of adsorbate directly in contact with the mesoporous film to analyze. This procedure eliminates the dead volume effect of the analysis chamber always encountered with pressurized techniques. In addition, the flux in itself helps the rapid equilibration at low

(13) Cagnol, F.; Grosso, D.; Soler-Illia, G. J. d. A. A.; Crepaldi, E. L.; Babonneau, F.; Amenitsch, H.; Sanchez, C. *J. Mater. Chem.* **2003**, *13*, 61−66.
(14) Klotz, M.; Albouy, P.-A.; Ayral, A.; Ménager, C.; Grosso, D.; van der Lee, A.; Cabuil, V.; Babonneau, F.; Guizard, C. *Chem. Mater.* **2000**, *12*, 1721.
(15) Gibaud, A.; Grosso, D.; Smarsly, B.; Baptiste, A.; Bardeau, J. F.; Babonneau, F.; Doshi, D. A.; Chen, Z.; Brinker, C. J.; Sanchez, C. *J. Phys. Chem. B* **2003**, *107* (25), 6114.
(16) Lu, Y.; Ganguli, R.; Drewien, C. A.; Anderson, M. T.; Brinker, C. J.; Gong, W.; Guo, Y.; Soyez, H.; Dunn, B.; Huang, M. H.; Zink, J. I. *Nature* **1997**, *389* (6649), 364.
(17) Besson, S.; Gacoin, T.; Jacquiod, C.; Ricolleau, C.; Babonneaud, D.; Boilot, J.-P. *J. Phys. Chem. B* **2000**, *104*, 12095.
(18) Crepaldi, E. L.; Soler-Illia, G. J. d. A. A.; Grosso, D.; Cagnol, F.; Ribot, F.; Sanchez, C. *J. Am. Chem. Soc.* **2003**, *125*, 9770.
(19) Grosso, D.; Cagnol, F.; Soler-Illia, G. J. d. A. A.; Crepaldi, E. L.; Amenitsch, H.; Brunet-Bruneau, A.; Bourgeois, A.; Sanchez, C. *Adv. Funct. Mater.* **2004**, *14* (4), 309.
(20) Grosso, D.; Boissiere, C.; Smarsly, B.; Brezesinski, T.; Pinna, N.; Albouy, P. A.; Amenitsch, H.; Antonietti, M.; Sanchez, C. *Nat. Mater.* **2004**, *3*, 787.
(21) Falcaro, P.; Grosso, D.; Amenitsch, H.; Innocenzi, P. *J. Phys. Chem. B* **2004**, *108* (30), 10942.

relative pressure by enhanced gas convection.[22] Though, working at atmospheric pressure limits the choice of efficient adsorbates for EEP measurements. Indeed, with atmosphere molecules being a huge majority in the gas flux, we had to select a chemical compound at the same time volatile at ambient temperature and presenting an affinity with silica strong enough to neglect the adsorption competitions at the surface of mesopores. Here we used water as the adsorbate considering its well documented affinity for silica surfaces.[10,11,23−25] For measurement, the cell temperature was fixed at 23 °C and was continuously filled by 2.5 L/min flux of air with a controlled water partial pressure.

Experimental Protocol of EEP Analysis. Typically, the ordered porous structure characterization method described in this article was performed in 4 steps, aiming at the determination of pores anisotropy, the plotting of a water adsorption−desorption isotherm of the mesoporous film, and the calculation of its porous parameters (porous volume, pore anisotropy, and size and surface area). The uniaxial young modulus (direction orthogonal to the substrate) was extracted from these results, as described in the discussion.

Step I: Determination of Pores Anisotropy. It consists of the preparation at ambient temperature of two films, the organic/inorganic mesostructured film, and a reference film prepared in the same conditions but containing no structuring agent. The reference film optical properties were assumed identical to those of silica walls of the mesostructured films. Optical constants of both films were determined by ellipsometry (in dry atmosphere), and the mesostructure organization was characterized by 2D-SAXS. An identical thermal treatment was then applied on both films, as detailed here after. The reference film was used to simulate the contraction behavior of the silica walls of the mesoporous network. Upon heating, spherical pores of the hybrid film flatten and become ellipsoidal. Final contractions of reference and mesostructure films were then determined by ellipsometry and used for the calculation of pores anisotropy via the isotropic inorganic contraction model which separates contraction contributions of the silica matrix and the mesostructure (vide infra the theoretical section).

Step II: Film Porous Volume and EEP Isotherm Determinations. The optical method used for the porous volume and isotherm determinations is usually based on the Lorentz−Lorentz equation which uses the optical index of the film analyzed and requires the macroscopic polarizability and molar volume of the adsorbed molecule.[5] In this work, the use of water as adsorbate in mesopores made the usual macroscopic description of water unreliable. Indeed, many works on water confining showed that highly curved water interfaces or confined water droplets have density, surface tension, and hydrogen bond network differing significantly from that of the bulk.[11,12,26,27] To overcome this problem, we calculated the volume of water adsorbed into the porous network with the Bruggemann effective medium approximation (BEMA) model, sometimes referred to as coherent potential approximation (eq 1). It allowed the determination of the relative volumetric fractions f_A and f_B of two materials A and B of known dielectric constants $\tilde{\epsilon}_A$ and $\tilde{\epsilon}_B$ within a volume unit of measured dielectric constant $\tilde{\epsilon}$. This equation takes into account the complex expression of the refractive index and is very accurate for a two component system

$$f_A \frac{\tilde{\epsilon}_A - \tilde{\epsilon}}{\tilde{\epsilon}_A + 2\tilde{\epsilon}} + f_B \frac{\tilde{\epsilon}_B - \tilde{\epsilon}}{\tilde{\epsilon}_B + 2\tilde{\epsilon}} = 0 \qquad (1)$$

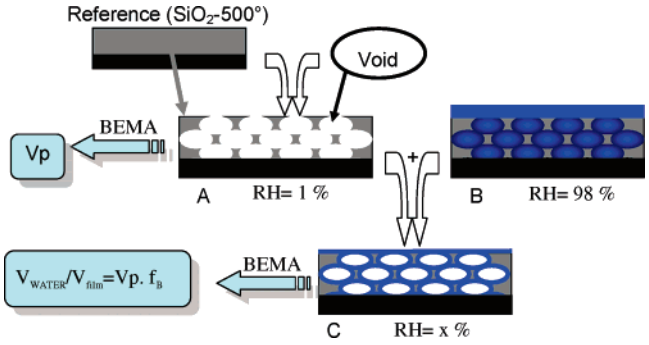

Figure 2. The A film porous volume V_p is determined by fitting with BEMA the volumetric fraction of void and reference film of the dry stabilized mesoporous film. V_{water}/V_{film} adsorbed is determined by fitting with BEMA the volumetric fraction of the dry stabilized mesoporous film A and the water saturated mesoporous film B.

The porous volume V_p of the mesoporous layer (measured in dry atmosphere) was determined with the BEMA by fitting the volumetric fractions of air and the silica matrix (which optical properties were obtained from the measurement of the reference film in step I) within the mesoporous film (Figure 2). The evolution of film refractive index n and thickness d as a function of the relative humidity (RH), $n = F(\mathrm{RH})$, and $d = F(\mathrm{RH})$, were measured by EEP. The adsorption−desorption isotherm $V_{WATER}/V_{FILM} = F(\mathrm{RH})$ was then determined with the BEMA by fitting the $n = F(\mathrm{RH})$ curve at each RH in order to determine volumetric fractions f_B of the water-saturated mesoporous film B and f_A of the dry mesoporous film. V_{WATER}/V_{FILM} was then assumed to be equal to the product of the porous volume and the volumetric fractions of the water-saturated mesoporous film (eq 2)

$$V_{WATER}/V_{FILM} = f_B V_p \qquad (2)$$

Step III: EP Determination of Water Layer Thickness Adsorbed at Each RH. This step allowed the determination of the thickness of water t adsorbed onto a flat surface of a reference SiO_2 film, assumed to give equivalent adsorption behavior than mesopores surface. t is directly measured by ellipsometry at each RH to produced the $t = F(\mathrm{RH})$ isotherm which is needed for the pore size determination in Step IV.

Step IV: Isotherm Analysis, Porous Network, and Mechanical Characterization. The pore size distribution (PSD) was determined from the isotherm obtained in Step II via a modified Kelvin equation taking into account the pore anisotropy (Step I) and the water layer thickness t (Step III). The film surface area was obtained via a t-plot treatment of the isotherm. Finally, the orthogonal Young modulus of the mesoporous film was extracted from the $d = F(\mathrm{RH})$ experimental curve via a combination of the Young-Laplace and the modified Kelvin equations (3) and (4) of the theoretical section.

Theoretical Section

Volumetric Pore Size Determination. The pore size determination was based on the Kelvin equation (3) which gives the relation between the relative pressure P/P_0 of an adsorbate, the liquid−air surface tension γ of a curved interface,[28] and the adsorbate liquid−interface surface area variation dS, when the volume V of adsorbate evolves of dV.[11,29] θ is the solid/liquid wetting angle, and V_L is the molar volume of the adsorbate after capillary condensation. Considering that metal oxide surfaces adsorbs very preferentially water to air molecules (N_2, O_2, and CO_2),

(22) This effect is assumed not disturbing the capillary condensation phenomenon attending that the air flow on top of the film is laminar (circulation speed within the analysis chamber is 8 cm/s) and that the very small pressure of the air flux onto the film surface is negligible if compared with capillary pressure difference taking place within the film during the water condensation.

(23) Llewellyn, P. L.; Schüth, F.; Grillet, Y.; Rouquerol, F.; Rouquerol, J.; Unger, K. K. *Langmuir* **1995**, *11*, 574.
(24) Cauvel, A.; BruneI, D.; Di Renzo, F. *Langmuir* **1997**, *13*, 2773.
(25) Yanagisawa, N.; Fujimoto, K.; Nakashima, S.; Kurata, Y.; Sanada, N. *Geochim. Cosmochim. Acta* **1997**, *61* (6), 1165.
(26) Smirnov, P.; Yamaguchi, T.; Kittaka, S.; Takahara, S.; Kuroda, Y. *J. Phys. Chem.* **2000**, *104*, 5498.
(27) Tolman, R. C. *J. Chem. Phys.* **1949**, *17* (3), 333.

(28) Modified accordingly to the Tolman model to take into account the decrease of surface tension due to the high curvature of liquid interfaces in mesoporous networks.

(29) Galarneau, A.; Desplantier-Giscard, D.; Dutarte, R.; Di Renzo, F. *Microporous Mesoporous Mater.* **1999**, *27*, 297.

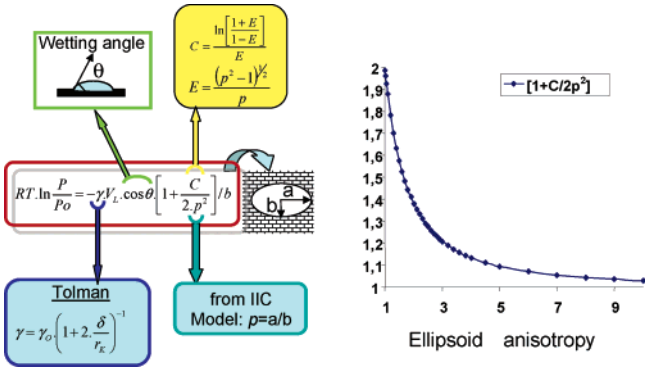

Figure 3. Kelvin equation modified for spherical ellipsoid pores, taking into account Tolman correction of the water surface tension for highly curved domains and the pore anisotropy p given by the IIC contraction model. The resulting geometric factor as a function of pore anisotropy is represented.

we assumed that the RH is equal to the partial pressure P/P_0 of the Kelvin equation

$$RT \ln \frac{P}{P_0} = \gamma V_L \cos \theta \frac{dS}{dV} \tag{3}$$

The Kelvin equation (4) was calculated for spheric−ellipsoidal pores of anisotropy p (where $p = a/b$, is the ratio of the ellipse large radius a on small radius b)

$$RT \ln \frac{P}{P_0} = -\gamma V_L \cos \theta \left[1 + \frac{C}{2p^2}\right]/b \tag{4}$$

with

$$C = \frac{\ln\left[\frac{1+E}{1-E}\right]}{E}$$

and

$$E = \frac{(p^2-1)^{1/2}}{p}$$

the eccentricity factor.

A similar calculation for a cylindrical interface is reported in Appendix I with the demonstration of eq 4. The representation of the geometric coefficient $G = [1 + C/2p^2]$ (Figure 3) as a function of the anisotropy p highlights that the Kelvin radius determination is very sensitive to the value of p, especially when it ranges between 1 and 3. A p value of 1 (case of a spherical interface) gives back the well-known Kelvin geometric factor G of 2. Interestingly, if the p value increases up to 3, G decreases down to 1.21, changing dramatically the calculated value of the pores small diameter b. Obviously, one meets here a problem of pore size determination as the Kelvin relation (4) contains two unknown parameters, b and p. To solve this problem, we determined the pore anisotropy with a pore contraction model named isotropic inorganic contraction (IIC; Figure 4). When p is known, the pore small radius can be calculated by adding the Kelvin radius b to the thickness t of the water layer adsorbed at the RH of the capillary condensation: b(pore) = b(Kelvin) + t.[11] Hereafter, we propose a simple model describing the contraction of amorphous metaloxide-based films, aimed at the prediction of the final anisotropy of the mesopores and based on film thickness values before and after calcination.

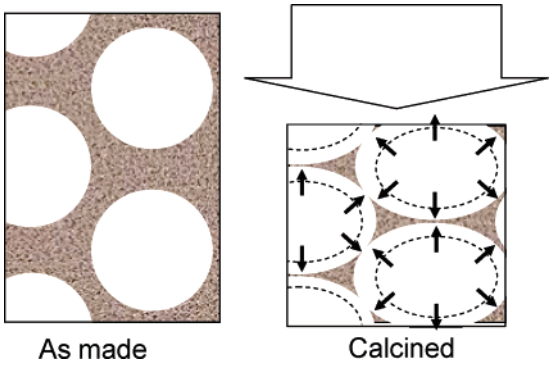

Figure 4. IIC lattice contraction model description. Black arrows represent the contraction directions of inorganic walls.

Isotropic Inorganic Pore Contraction (IIC) Model. The IIC model is based on the hypothesis that the contraction of mesostructured films can be described by an ellipsoidal contraction of pores resulting from the contraction of the mesostructure lattice, plus a simultaneous isotropic contraction of silica walls between mesodomains (Figure 4). The isotropic walls contraction is assumed to be equal to the uniaxial contraction of the reference film at the power 1/3. The IIC model is supported by the fact that, contrary to pure silica reference films in which silica contraction can only be macroscopically relaxed in the direction normal to the substrate, in mesostructured films, the in-plane contraction may be locally relaxed by the deformation of the mesopores. The anisotropy parameter p can then be obtained in a very simple way by the eq 5 in which $d_{\mathrm{FILM\ T}}$ and $d_{\mathrm{REF\ T}}$ are thicknesses of mesostructured and reference films obtained by ellipsometry at the temperature T. The same anisotropy parameter can be obtained if $d_{\mathrm{FILM\ T}}$ values are the d spacing values obtained from XRD experiments in Bragg Brentano geometry

$$p = \frac{d_{\mathrm{FILM\ 25}}}{d_{\mathrm{FILM\cdot T}}}\left(\frac{d_{\mathrm{REF.T}}}{d_{\mathrm{REF\ 25}}}\right)^{1/3} \tag{5}$$

Finally, the IIC model does not imply that the reference film contraction has to be inferior or equal to the mesostructured film contraction. Hence, it can be used to describe mesodomains flattening whatever the calcination temperature, before or after the removal of structuring agents.

Results and Discussion

Two types of mesoporous films with cubic ordered mesodomains were prepared by the EISA method following previously reported protocols. They were analyzed by ellipsometry and 2D-SAXS and heated at 100 °C for one night before any further treatment. TEM pictures of these mesostructures are given in Figure 5. 2D-SAXS experiments (not shown here) confirmed the cubic space group of CS-25 with a $Pm3n$ symmetry and of FS-25 with a $Im3m$ symmetry.[13,21] Diffraction spots assignment evidenced that, in the as-made films, both mesostructures are noncontracted.

Study of Films Contraction during Calcination. As reported in the literature, structuring agents are commonly removed by calcination at a temperature equal to or higher than 500 °C. Upon calcination in air from 100 to 500 °C (5°/min gradient), ellipsometry and 2D-SAXS analyses showed that films constantly shrink in the direction perpendicular to the substrate. For mesostructured frameworks, the isotropic lattice contraction, well

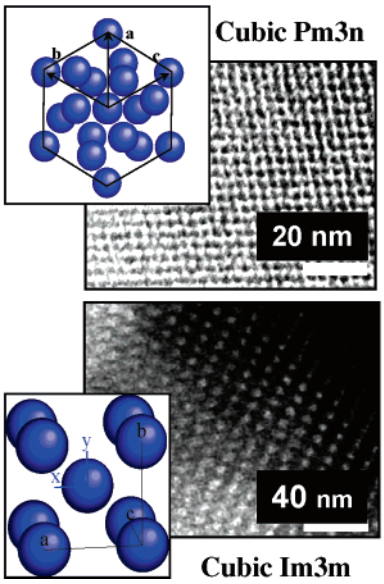

Figure 5. TEM pictures of silica films prepared with CTAB and F127 structuring agents after heat treated at 100 °C. Insert: simplified *Pm3n* structure of as made CTAB films and *Im3m* structure of as made F127 films.

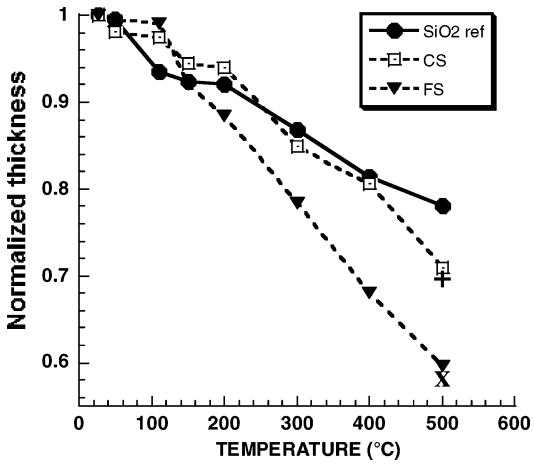

Figure 6. Pure SiO2, CS and FS film contractions with temperature obtained from ellipsometry measurements. (×) FS-500 and (+) CS-500 contractions obtained by LAXRD and SAXS analyses (from refs 20 and 27).

documented for the calcination of analogous powders, was for a large part due to the water loss and to the condensation of the silica network.[30] The evolution of films thicknesses as a function of calcination temperature, reported in Figure 6, showed that the reference SiO_2 film contracted more than hybrid ones at low temperature (T < 150 °C), but less above 200 °C. This behavior is due to the presence of the amphiphilic molecules in hybrid films which volume is fixed (neglecting thermal dilatation) from ambient temperature up to the decomposition temperature (starting at 150 and 250 °C respectively for F127 copolymer and CTAB). At low temperature, the hybrid films contraction is thus limited to the volumetric contraction of their silica fraction. At temperatures higher than 200 °C, the thickness decrease is cumulatively due to the contraction of silica walls and porous uniaxial structure contraction in the direction orthogonal to the substrate. The final contractions at 500 °C, reported in Table 1, are 21.9%, 29%, and 40.4% respectively for reference films SiO_2, CS-500, and FS-500.

Table 1. Contraction Silica Films with Calcination Treatment

(/nm)	CS thickness	FS thickness	simple SiO_2 film thickness	CS GI−SAXS	FS GI−SAXS
25 °C	239.8	186.7	63.9		
500 °C	170.3	111.3	49.9		
contraction rate	29.0%	40.4%	21.9%	≈30%	≈42%

Monitored by 2D-SAXS, this macroscopic contraction was shown to be concomitant with a progressive contraction of the mesostructures in the direction orthogonal to the substrate. Deformation of original cubic lattices of CS and FS films were observed along the [211] and [110] directions respectively, and no in-plane contraction (parallel to the substrate) was observed. Finally, with films macroscopic contractions and mesostructures contractions values (Table 1) being very close, we concluded that mesostructure lattice contractions of silica mesoporous films can be quantified with a good accuracy by a simple ellipsometric monitoring of films thicknesses. We assumed in this article that this uniaxial contraction induced a transformation of the pores from spherical to ellipsoidal shape.

The IIC model, detailed in the theoretical section, describes the film contraction as the result of the uniaxial pores flattening and the silica wall isotropic contraction. Hence, the thicker the silica wall in one direction, the wider the pore dimension increases in this direction. For FS-500 films, the *Fmmm* final symmetry group of the contracted mesostructure implies that the ellipsoidal shape of pores tends to become a truncated and contracted octahedron.[21] On the other hand, in CS-500 films, the contraction of the *Pm3n* symmetry along the [211] direction leads to two different pore environments. A quarter of the pores present a "flattened" icosahedral deformation, and a complex nonisotropic transformation occurs for the others. Therefore, describing the pore geometry with high precision is only possible with computational modelisation. In this work, we assumed that the final dS/dV expression of the Kelvin equation of the real pores shape does not differ significantly from the ellipsoidal geometry.

The anisotropy factor calculated for the SF-500 film was equal to 1.55 (leading to a G value of 1.55), whereas the anisotropy factor calculated for the CS-500 film was 1.33 (leading to a G value of 1.71). Hence, a significant pore deformation was observed after calcination at 500 °C for both mesostructures. In these cases, the anisotropy correction of the Kelvin equation allowed corrections of the pore size values as high as 24.7% if compared with a simple spherical pores model. Therefore, pore size contraction is in no way a negligible parameter and will be of paramount importance, especially for pore size determination of non-silica films whose contractions are much higher than contractions of the present silica films. Another example of the tremendous influence of pores anisotropy was recently published. This publication describes a γ-Al_2O_3 nanocrystallized mesoporous film for which pores anisotropy value was as high as 4. In this case, the G factor of the Kelvin equation became 1.13; thus, the present pore size determination approach corrected the measured pore size value by nearly 44%.[31]

(30) Innocenzi, P.; Falcaro, P.; Grosso, D.; Babonneau, F. *J. Phys. Chem. B* **2003**, *107* (20), 4711.

(31) Kuemmel, M.; Grosso, D.; Boissiere, C.; Smarsly, B.; Brezesinski, T.; Albouy, P. A.; Amenitsch, H.; Sanchez, C. *Angew. Chem.* **2005**, *44*, 4589.

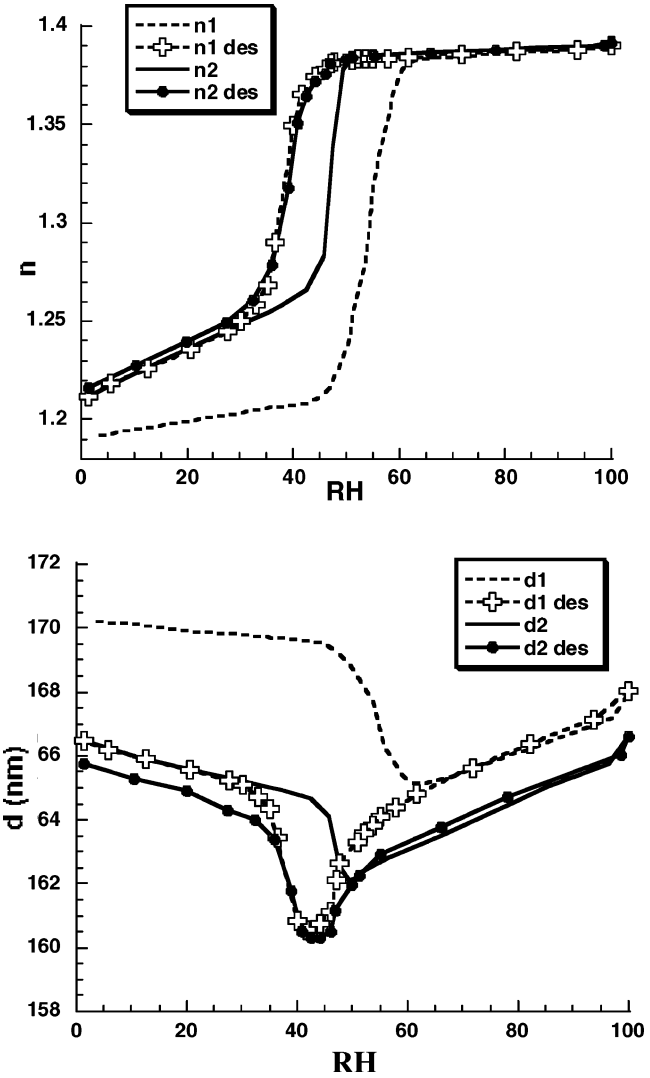

Figure 7. Evolutions of optical index n and film thickness d of the CS-500 film as a function of RH of two water subsequent adsorption−desorption cycles.

EEP Analysis of the CS-500 Film. The ellipsometric measurements of the refractive index n and thickness d of a CS-500 film were carried out at different RHs of water (reported in Figure 7). Two adsorption−desorption cycles were performed on each film in order to investigate the stability of the films and the rehydration of the silica surfaces.

The first isotherm exhibited a low value of refractive index at low RH ($n_{700\ nm} = 1.19$), which is characteristic, for silica, of the presence of a large fraction of micro and/or mesopores within a silica film.[5,9] With the increasing of RH, very little adsorption was observed up to a RH of 45%. At higher RH, a steep increase of refractive index was observed, characteristic of mesopores filling of water by capillary condensation. After the first adsorption−desorption cycle, the refractive index at low RH was higher than the original one. This was partly due to a densification of the film induced by the capillary stress produced during the water condensation into mesopores and partly due to the chemisorption of additional matter within the porous network (as checked by FTIR measurements in dry air, not shown here).[10,26,32] With the first isotherm, the CS-500 film contracted irreversibly from 170.3 to 166.5 nm.

(32) Inagaki, S.; Fukushima, Y. *Microporous Mesoporous Mater.* **1998**, *21*, 667.

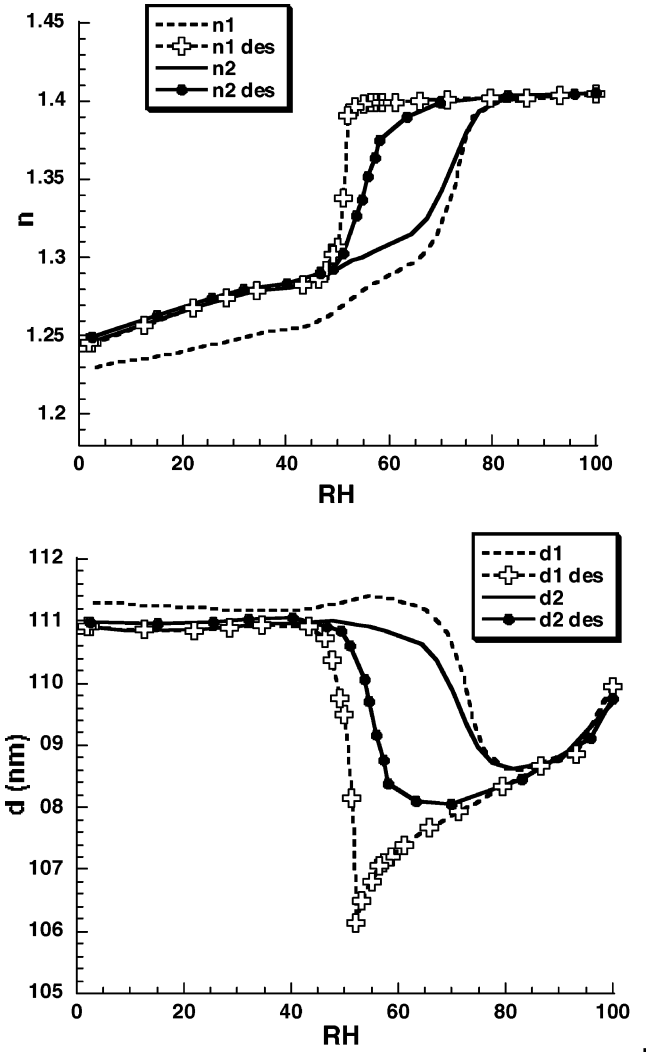

Figure 8. Evolutions of optical index n and film thickness d of the FS-500 film as a function of RH of two subsequent water adsorption−desorption cycles.

A second adsorption−desorption cycle produced a reversible isotherm with a refractive index n_{700} value of 1.25 at low humidity. A negligible irreversible contraction of the film was observed (<0.5% for the second isotherm). Both isotherms $n = F(\text{RH})$ desorption branches were similar, attesting that the only important modification of the film was water chemisorption of the first adsorption cycle. The capillary condensation taking place at lower RH during the second adsorption−desorption cycle confirmed the water chemisorption. This phenomenon is a consequence of the lowering of the water-on-silica wetting angle induced by the rehydration of the silica surface. This effect is described by the Kelvin equation which predicts, for the same pore size, different capillary absorption P/P_0 values when the wetting angle evolves.[11,32] Finally, one could conclude that, the first adsorption−desorption cycle stabilized the CS-500 film versus capillary stress and water composition.

EEP Analysis of the FS-500 Film. Two water adsorption−desorption cycles were performed on SF4-500 films (Figure 8). The first cycle promoted an irreversible increase of refractive index, resulting from the irreversible chemisorption of water within the structure, in good accordance with IR ellipsometry measurements.[10] Here, a very small irreversible uniaxial contraction of the film (0.3%) was observed. During the first capillary desorption, the decrease of the optical index was very steep at RH =

52% (but taking place at higher relative humidity than in the CS-500 system, it was not interpreted as a critical desorption resulting from the water meniscus instability). In the second cycle, the capillary desorption began at RH higher than 70%. Assuming that pore geometry was the same for both cycles, this large difference of RH resulted very probably from a variation of pore size, i.e., smaller pores at the first desorption than at the second one. This interpretation was asserted by the fluctuation of film thickness during desorptions. Indeed, the capillary desorption of the first cycle promoted significant contraction of the film and a sudden asymptotical like break at RH = 52%, followed by the rapid relaxation of the capillary stress applied in the direction perpendicular to the substrate. During the capillary desorption of the second cycle, one observed that the film contracted continuously and relaxed continuously at a higher RH value than during the first cycle. We concluded that, in SF-500 films, the first desorption of water promoted the destruction of the brittle parts of the mesoporous network which resulted in enlarging bottleneck windows joining ellipsoidal mesopores with each other. Hence, the first adsorption−desorption cycle led to a stabilization of the mesostructure versus water stress by promoting not only the rehydration of the silica surface but also the widening of the connectivities of mesopores.

Volumetry Analyses of Stabilized Mesoporous Films. All volumetry analyses were performed on already stabilized films, i.e., on data collected during the second adsorption−desorption experiment. Porous volumes of CS-500 and FS-500 films were measured via the BEMA at 0.47 and 0.40 cm^3/cm^3, respectively. The data analysis approach we used assumes the chemisorbed water to be a part of the silica wall. Hence, in the following experiments, we only measured the volume of water physisorbed into the pores. As a consequence, any small microporosity filled with chemisorbed water or closed porosity was masked or out of reach of the EEP analysis. The beneficial counterpart of this approach was a strict limitation of approximations made on optical properties of films.

For the reconstruction of the $V_{WATER}/V_{FILM} = F(RH)$ isotherms, we assumed that, at each point of the isotherm, the film could be described by a material in which the optical properties are a mixture of the film optical properties at the lowest RH and the same film optical properties when all mesopores are filled with water (after capillary condensation). With such a hypothesis, water optical properties were not taken from tabulated values but experimentally measured in confined medium and reused in a self-consistent BEMA model. The obtained $V_{WATER}/V_{FILM} = F(RH)$ isotherms are shown in Figure 9. Both isotherms were characteristic of isotherms observed for mesostructured powders with steep steps of adsorption near RH of 50% and 72% respectively for CS-500 and FS-500 films. The absence of an additional adsorption step at high RH was due to the perfectly flat surface of the films. Pore size distributions obtained with the IIC modified Kelvin model are reported in the Table 2. Calculated pores anisotropies were 1.33 and 1.56 respectively for CS-500 and FS-500 films when the contraction induced by the first isotherm is taken into account (with final Kelvin G factors of 1.68 and 1.55). Finally, to complete the Kelvin equation, we measured the water−silica wetting angle θ equal to 27°, as calculated by Inagaki et al. on mesoporous silica powders[32] for identical experimental adsorption conditions. Pore size distributions (PSD), shown in Figure 10, are narrow and allow the direct measurement of ellipsoid pore dimensions from the adsorption and pore restrictions from the desorptions. Pore

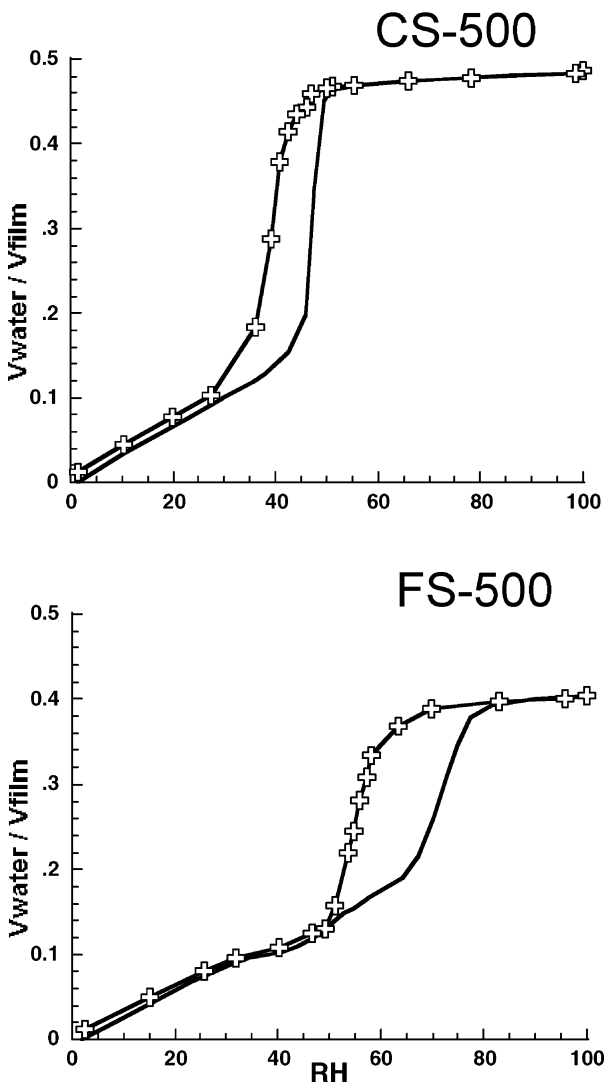

Figure 9. Adsorption desorptions isotherms of stabilized CS-500 and FS-500 films obtained from the BEMA model.

restrictions are openings joining pores in the direction of the smallest distance between ellipsoidal pores. In our films, the nearest mesopores are neither superimposed nor coplanar with respect to the substrate plane, hence restrictions geometry is unlikely to be cylindrical (cf. Supporting Information). In the first approximation, the PSD given here was calculated by assuming an identical anisotropy factor for pores and pore restrictions. Large dimensions of ellipsoid pores obtained were 2.4 and 6.4 nm respectively for CTAB and F127 systems. These values are consistent with pore size measured on their mesoporous powder counterparts by nitrogen porometry and other mesoporous films by EP with organic solvents (pore were assumed spherical in the latter case).[9,33−35]

For both isotherms, the BET equation failed to give coherent estimation of surface areas when water was adsorbed. Hence, we replaced the BET method by a t-plot analysis (Figure 11). Surface area value S could be obtained from the measurement of slopes β of the t-plot

(33) Morey, M. S.; Davidson, A.; Stucky, G. D. *J. Porous Mater.* **1998**, *5* (3/4), 195.
(34) Kruk, M.; Jaroniec, M.; Ryoo, R.; Ryoo, R.; Kim, J. M. *Chem. Mater.* **1999**, *11*, 2568.
(35) Rathod, S.; Rao, G. V. R.; Andrzejewski, B.; Lopez, G. P.; Ward, T. L.; Brinker, C. J.; Datye, A. K. *Mater. Res. Soc. Symp.* **2003**, *775*?, 15.

Table 2. Geometric Description of FS-500 and CS-500 Films (IIC Model)

	pore contraction	small diameter[a] (nm)	large diameter[a] (nm)	desor. small diameter[a] (nm)	desor. large diameter [a] (nm)	porous volume (cm^3/cm^3)	mesoporous surface (m^2/cm^3)		
FS	35.7%	4.5	6.4	2.8	3.4	0.33 + 0.7[b]	339[c]	377[d]	214[e]
CS	24.7%	1.9	2.4	1.5	1.9	0.47		720[d]	231[e]

[a] After addition of the water multilayer thickness. [b] Microporosity. [c] Geometric surface. [d] *t*-plot surface by slope ratio. [e] Direct *t*-plot surface.

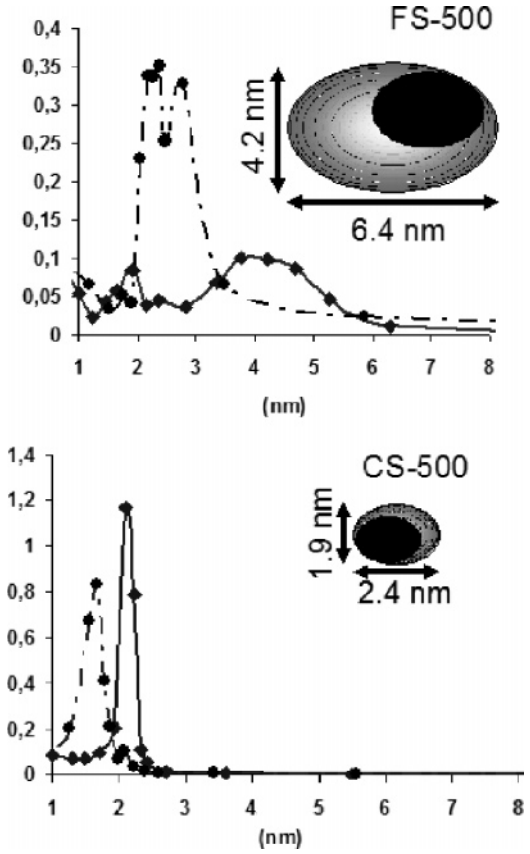

Figure 10. Ellipse small axis size determinations of FS-500 and CS-500 films with the IIC contraction model from (—) adsorption and (- - -) desorptions parts of isotherms. In the insets are represented in gray the pore aspect ratio and size deduced from adsorption and in black desorptions. Pore anisotropy was assumed identical at adsorption and desorption.

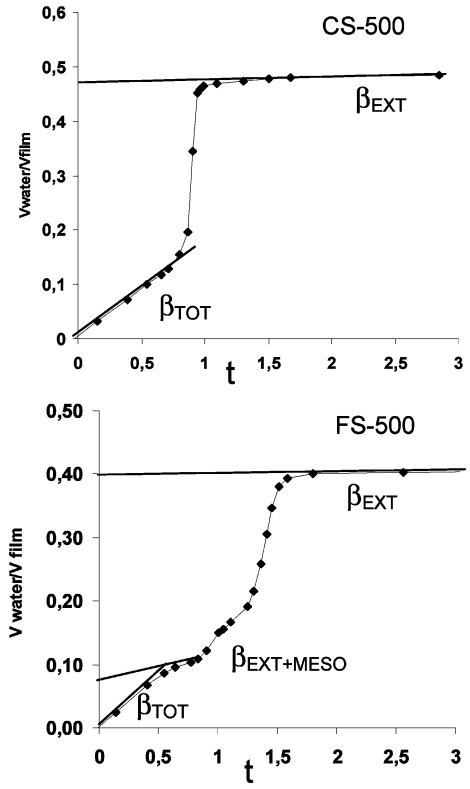

Figure 11. Plot of the adsorbed water volume as a function of water film thickness *t* in angstroms.

curve and eq 6 in which ρ_L and ρ_G are densities of the adsorbate in liquid and gas states

$$S = \frac{\rho_L}{\rho_G} \cdot \beta \tag{6}$$

The slope β_{EXT} at high RH gives the external surface area S_{EXT} (corresponding to the external surface of films), and the slope β_{TOT} at low RH gives the total surface area S_{TOT} (porous network surface plus external surface). From β_{TOT}, we obtained CS-500 and FS-500 surface areas of 231 and 214 $m^2 \cdot cm^{-3}$ respectively. We noticed here that these surface values are very probably heavily underestimated because of a large uncertainty on the tabulated values of ρ_G[36] and ρ_L of water in our experimental conditions. Another way to obtain S_{TOT} consists of extracting the mesoporous surface area from the ratio of external surface area (which is accurately known from the film thickness) and the total surface area, as shown in eq 7

$$S_{TOT} = S_{EXT} \frac{\beta_{TOT}}{\beta_{EXT}} \tag{7}$$

Surface area values obtained by this way (reported in Table 2) were 720 and 377 $m^2 \cdot cm^{-3}$ for CS-500 and FS-500 films, respectively. Here, again, an uncertainty (about 20−40%) still exists because the β_{EXT} value is always very small for films and thus difficult to measure with a good accuracy. For comparison, a geometric surface area was calculated from the total mesoporous volume and mesopores dimensions, from which was removed the contribution of pores restrictions. This calculation required the knowledge of the mean number of connections between pores. The latter method is only reliable if these connections are of the size measured from the desorptions branch of isotherms. These conditions were fulfilled for the FS-500 film (4 connections/pore resulting in the *Im*3*m* mesostructure contracted along the [110] direction, cf. the Supporting Information). The geometrical surface area was 339 $m^2 \cdot cm^{-3}$. Unfortunately, a similar calculation could not be done for the CS-500 films considering that several pore environments exist and, thus, that pores connectivities of different sizes exist.

(36) Plyasunov, A. V.; Shock, E. L. *J. Chem. Eng. Data* **2003**, *48*, 808.

Finally, pore size distribution of the mesoporous silica films investigated could be calculated with a good precision by coupling the Kelvin equation and the IIC contraction model. Surface area values obtained by different methods (*t*-plot or geometric) were coherent with those observed for mesoporous powders prepared in similar ways. Yet, these values were spread in a large range, mainly because their determination on films with water is model dependent or because of large experimental errors promoted by the adsorbate and the intrinsic geometry of the films. However, qualitative comparisons of samples surfaces were still possible by using eq 6.

Young Modulus Calculation. Mechanical properties of supported porous thin films are of paramount importance for numerous high technology applications such as ultralow-*k* films, membrane science, or sensing. So far, only a few techniques allow the measurement of Young's modulus *E*, essentially nano indentation (NI), surface acoustic waves spectroscopy, and Brillouin light scattering. NI is the most common in laboratories but overestimates chronically Young's modulus of thin films due to the influence of the rigid substrate. A nondestructive alternative was reported by Mogilnikov and Baklanov in 2002 which allows the determination of Young's modulus by analysis of film thickness evolution during EP measurements.[37] By coupling the expression of the Kelvin and Young−Laplace equations, they obtained a model describing the evolution of the film thickness when capillary stress reversibly contracts the film (that is, when the stress promotes a deformation within the elastic deformation domain). This expression (eq 8) links the film thickness d_i at fixed partial pressure P_i/P_0, the unstressed film thickness d_0, the Young's modulus E, and the microscopic capillary pressure π_i across the liquid−air interface

$$d_i = d_0(1 - \pi_i/E) = d_0 + k \ln\frac{P_i}{P_0} \qquad (8)$$

The k variable being dependent on the Kelvin equation, it can be expressed for different pore geometries. If coupled with the IIC model of contraction and modified Kelvin equations (4), one obtains a new expression of E (eq 9) in which p is the anisotropy of ellipsoidal pores, G is the geometric factor of the modified Kelvin equation, and V_L is the molar volume of the adsorbate. The fit of $d_i = F(P_i/P_0)$ gives the value of k and allows for the determination of E

$$E = \frac{d_0 RT}{V_L \cos\theta}\frac{(1+p)/p}{G}\frac{1}{k} \qquad (9)$$

According to the literature, such a fit method is successful when applied to xero gel thin films on which capillary condensation promotes monotonic thickness decrease and increase.[37] On the other hand, thickness variations of our mesostructured films clearly exhibit three different behaviors (Figure 12). A low RH zone I before capillary condensation with a monotonic thickness variation and the capillary condensation zone II with a steep thickness decrease corresponding to the sudden filling (emptying) of mesopores and the appearance (disappearance) of a true liquid meniscus, and a zone III in which the curvature of the liquid meniscus decreases (increases) continuously. No Young's modulus can reasonably be determined from zone I with eq 10 as, at low RH; only the few molecules of water already adsorbed do not behave like a liquid.

(37) Mogilnikov, K. P.; Baklanov, M. R. *Electrochem. Sol. Stat. Lett.* **2002**, *5* (12), F29.

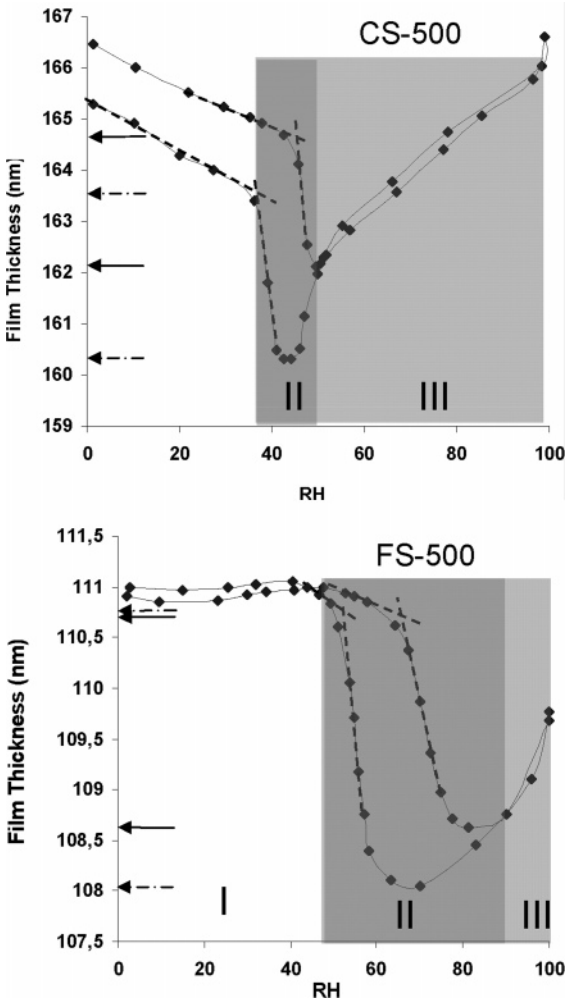

Figure 12. Film thicknesses of CS-500 and FS-500 films. Zone I: monomultilayer adsorption of water; zone II: capillary condensation of water within mesopores. From this zone, E can be obtained by direct measurement of the contraction by using eq 10; zone III: progressive relaxation of the capillary stress. From this zone, E can be obtained by direct fitting of $d = F(P/P_0)$ with eq 9.

Zone III is typically the domain in which a fit with eq 9 can be used for E calculation. In zone II, the fit procedure does not work, but a direct calculation of E can be made with eq 8 developed at capillary condensation RH point to obtain eq 10

$$E = \frac{\pi_C}{\Delta d/d_C} = \frac{\frac{\gamma}{b}\frac{(1+p)}{p}}{\Delta d/d_C} \qquad (10)$$

in which π_C is the microscopic capillary pressure when capillary condensation occurs. b is the ellipsoidal pore small diameter already measured by EEP, d_C is the film thickness before capillary contraction, Δd is the thickness variation induced by capillary condensation, and γ is the modified liquid surface tension according to Tolman.[27]

Both zones II and III were used to obtain E for the CS-500 film (Table 3). The E value obtained from the fit of several films was 4.78 ± 0.05 GPa whatever the geometric model used, in good accordance with values obtained from direct measurement of eq 10 at 4.48 ± 0.04 GPa. Contrarily to pore size or geometric surface, Young's modulus determination seemed to present very little dependence on the contraction of pores. This can be rationalized by the fact that pore anisotropy induces little

Table 3. Young's Modulus

/GPa	CS-500		FS-500	
E_{IIC} direct	4.52[a]	4.45[b]	1.45[a]	1.64[b]
E_{IIC} fit	4.78			

[a] From adsorption curve. [b] From desorption curve.

evolution of the geometric factor $(1 + p)/pG$ of eq 9. Eventually, the plot of this factor shows that the liquid−gas interface geometry (from spherical with $G = 2$ and $p = 1$, to cylindrical with $G = 1$ and $p = \infty$) has only a small influence on the determination of E and can be approximated to one for small pores anisotropy or near cylindrical pores. For intermediate anisotropy, between 1.4 and 15, this approximation underestimates the E values by 5−11%. By comparison, Young's modulus values measured by NI on similar films were much higher (15 GPa for CTAB films and 11 GPa for F127 films) but unreliable for layers of thickness inferior to 300 nm because the hard substrate contribution is difficult to separate from the film contribution.

For the FS-500 film, no fit could be performed on zone III because of the high pore size which restrains zone III of the contraction isotherm to a too small domain of RH. Obviously, eq 10 has to be favored when capillary adsorption takes place at high RH. Then, Young's modulus can only be obtained if the pore anisotropy is known. The direct measurement in zone II gave different E values between adsorption curve 1.45 ± 0.02 GPa and desorption curve 1.64 ± 0.03 GPa, that is, a mean E value of 1.54 ± 0.1 GPa. The higher rigidity of CS films is a trend already observed for mesoporous powders.[38] It can be rationalized by the fact that, despite thicker walls, pluronic block copolymer mesoporous films prepared at ambient temperature contain a higher microporous volume and a lower (wall thickness)/(cell parameter) ratio than CTAB films. Those two effects compromise the global cohesion of the rigid structure[38−40] if no stabilizing posttreatment is performed such as adsorption of volatile silicon alkoxide into micropores.[41] However, if compared with Young modulus of silica xerofilms obtained by EP technique, mesostructured materials still exhibit Young's modulus values much higher at identical total porous volume.[37]

Conclusion

We validated here for the first time that the EEP technique is able to perform simple, cheap, and accurate determination of PSD, porous volume, pore size, pore accessibility, and orthogonal Young's modulus of mesoporous thin films. The uniaxial contractions of two types of mesoporous thin films featuring contracted *Pm*3*n* and *Im*3*m* cubic mesophases were investigated by combination 2D-SAXS and/or EEP. We evidenced a homothetic relation between the film macroscopic contraction and the mesoscopic porous lattice contraction. We proved that the calculation of mesostructure contraction can be done easily by ellipsometry with no need of additional 2D-SAXS experiments. These contraction data were used to calculate the anisotropy of the mesopores via the IIC model. Coupled with a modified Kelvin equation, the IIC model allowed a precise pore size measurement, correcting classical models errors of about 25% in the presented examples. The recently published examples of mesoporous nanocrystalline γ-Al_2O_3 thin films showed that the theoretical approach developed in this article is even more important for large anisotropy factors ($5 > p > 3$). In these materials, the use of a spherical (or cylindrical) pores model induces errors higher than 40% on pore size determinations.[31] The exact value of p being the crucial point of the pore size determination, multiangle SAXS experiments are carried out at the moment in order to reconstruct accurately the shape and connectivities of porous networks of these films. These data will be used to confirm and further improve the actual contraction model.

Appendix I. Development of Kelvin Equation Modified for Ellipsoidal Pore Shapes

Kelvin Equation for Ellipsoidal Spheres.

$$RT \ln\frac{P}{P_0} = \gamma V_L \cos\theta \frac{dS}{dV} \tag{3}$$

Hereafter, we calculated the dS/dV factor for a pore with spheric-ellipsoidal shape of anisotropy p equal to the ratio of the ellipse large radius a on small radius b. The resulting ellipsoidal sphere volume and surface expressions are given as function of b and p in eqs 3′ and 3″, respectively

$$V = \frac{4}{3}\pi p^2 b^3 \tag{3'}$$

$$S = 2p^2 b^2 \pi + (\pi b^2/E) \ln\left[\frac{1+E}{1-E}\right] \tag{3''}$$

with

$$E = \frac{(p^2-1)^{1/2}}{p}$$

the eccentricity factor.

Reintroduced into eq 3, we obtain the Kevin equation for ellipsoidal interfaces:

$$RT \ln\frac{P}{P_0} = -\gamma V_L \cos\theta \left[1 + \frac{C}{2p^2}\right]/b \tag{4}$$

with

$$C = \frac{\ln\left[\frac{1+E}{1-E}\right]}{E}$$

Kelvin Equation for Ellipsoidal Cylinders. In the same way, the Kelvin equation can be modified to describe ordered mesopores with 2D hexagonal pore packing, contracted normally to the c axis of the hexagon. One obtains then the following equation in which b represents the small radius of the ellipsoidal section of a flatten cylinder:

$$RT \ln\frac{P}{P_0} = -\gamma V_L \cos\theta \left[\frac{1}{2}\left(1 + \frac{1}{p}\right)\right]/b$$

Supporting Information Available: Schematic representation of the FS-500 porous network resulting of the contraction of an *Im*3*m* mesostructure along the [110] direction. This material is available free of charge via the Internet at http://pubs.acs.org.

LA050981Z

(38) Galarneau, A.; Desplantier-Giscard, D.; Di Renzo, F.; Fajula, F. *Catal. Today* **2001**, *68*, 191.
(39) Galarneau, A.; Cambon, H.; Di Renzo, F.; Fajula, F. *Langmuir* **2001**, *17*, 8328.
(40) Galarneau, A.; Cambon, H.; Di Renzo, F.; Ryoo, R.; Choi, M.; Fajula, F. *New J. Chem.* **2003**, *1*, 73.
(41) Xiao, X.; Hata, N.; Yamada, K.; Kikkawa, T. *Rev. Sci. Instrum.* **2003**, *74* (10), 4539.